ACS Sustainable Chemistry & Engineering

Research Article

pubs.acs.org/journal/ascecg

Green Synthesized Silver and Gold Nanoparticles for Colorimetric Detection of Hg^{2+}, Pb^{2+}, and Mn^{2+} in Aqueous Medium

M. Annadhasan,[†] T. Muthukumarasamyvel,[†] V. R. Sankar Babu,[†,‡] and N. Rajendiran[†,*]

[†]Department of Polymer Science, University of Madras, Maraimalai Campus, Guindy, Chennai, Tamil Nadu 600 025, India

[‡]Metrohm India Limited, Thuraipakkam, Chennai, Tamil Nadu 600 096, India

Supporting Information

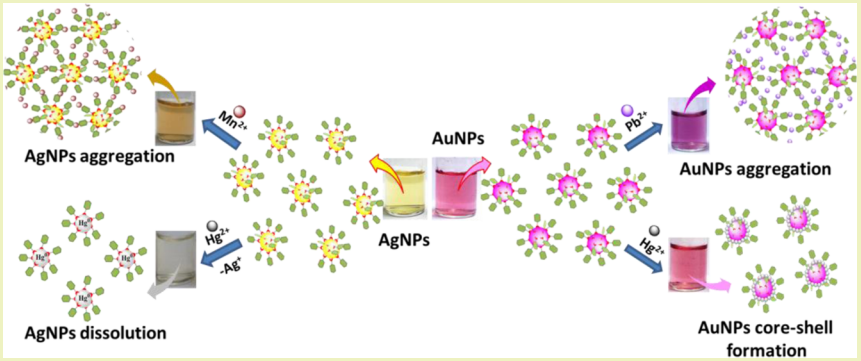

ABSTRACT: In this study, we report a simple and green method for the synthesis of L-tyrosine-stabilized silver (AgNPs) and gold nanoparticles (AuNPs) in aqueous medium under ambient sunlight irradiation. The nanoparticles (NPs) are characterized by UV−visible spectroscopy, high-resolution transmission electron microscopy (HR-TEM), Fourier transform infrared spectroscopy (FT-IR), cyclic voltammetry (CV), and dynamic light scattering (DLS) techniques. The size and shape of the metal NPs could be controlled by changing the concentration of the substrate, metal precursors, and pH of the medium. The synthesized AgNPs are found to be highly sensitive to Hg^{2+} and Mn^{2+} ions with the detection limit for both ions as low as 16 nM under optimized conditions. However AuNPs are found to be sensitive to Hg^{2+} and Pb^{2+} ions with a detection limit as low as 53 and 16 nM, respectively. The proposed method was found to be useful for colorimetric detection of heavy metal ions in aqueous medium.

KEYWORDS: *Green synthesis, L-Tyrosine, Silver nanoparticles (AgNPs), Gold nanoparticles (AuNPs), Sunlight irradiation, Colorimetric sensor, Heavy metal ions*

INTRODUCTION

Noble metal nanoparticles such as silver (AgNPs) and gold nanoparticles (AuNPs) have drawn remarkable interest in the past few years as they exhibit strong absorption of electromagnetic waves in the visible region due to surface plasmon resonance (SPR), highly stable dispersions, chemical inertness, and biocompatibility.[1,2] A small change in the NPs size, shape, surface nature, and distance between particles leads to tunable changes in their optical properties,[3,4] which find application in the fabrication of optical devices,[5] catalysis,[6] surface-enhanced Raman scattering (SERS),[7] bioimaging,[8] colorimetric sensors,[9] and so on. As a result of their uses in the biological and chemical applications, researchers were inspired to integrate "green chemistry" approaches to functionalize the AgNPs and AuNPs using biomolecules like carbohydrate,[10] proteins,[11] amino acids,[12] biopolymers,[13] etc. Few groups have focused on green synthetic pathways for nanomaterial's synthesis. Among them, the Varma et.al. group concentrated on green synthesis of noble metal nanoparticles using plant extracts, vitamins, biosurfactants, etc. in aqueous medium.[14−18] Ag−Au bimetallic NPs were made by Wallen et.al. using glucose and starch as reducing and stabilizing agents.[19] Plant tannin was used for synthesis of AuNPs.[20] Very recently, He and co-workers reported utilization of trypsin for green synthesis of AuNPs.[21]

Amino acids (AA) are usually classified different ways based on the polarity and nature of side groups, namely, weakly acidic or basic, hydrophilic, and hydrophobic. The physicochemical properties of the side groups are important because they can influence the reduction, stabilization, and conversion of reducible metal ions (Ag^{+}/Au^{3+}) to the NPs, respectively.[22] Thus, AA may serve as the effective precursor for the green synthesis of AgNPs and AuNPs. Many reports are documented for the synthesis of AgNPs and AuNPs using various amino acids and amino acid-modified amphiphiles as capping agents in the presence of different reducing agents as well as operating under various experimental conditions.[23−31] However, the

Received: December 3, 2013
Revised: January 29, 2014
Published: February 4, 2014

drawback of using additional reducing agents may complicate the recovery of the final products and also render them unsuitable for further biological or chemical applications. The other approaches cited in the literature require tedious multistep thermal treatment or sophisticated techniques for the synthesis of NPs.

There are many reports available for the synthesis of AgNPs and AuNPs using AA as the capping and reducing agents. Selvakannan et.al. reported synthesis of tryptophan-capped and reduced AuNPs in aqueous medium.[25] Shao et al. reported size- and shape-controlled synthesis of gold nanostructure using aspartate as reducing and capping agents.[32] Later, Ma et.al. reported one-pot synthesis cysteine-capped and reduced AuNPs in aqueous solution at room temperature.[33] Recently, Khan and co-workers reported on the synthesis of AgNPs using tyrosine, aspartic acid, and tryptophan as reducing and capping agents in the presence of surfactant as the shape-directing agent.[34−36] Suri et.al. reported synthesis of AuNPs using glutamic acid as a self-reducing agent.[37] Sastry et.al. reported synthesis of AuNPs using various AA as the capping agent.[38,39] A review also exists on the dual roles of compounds from plant extracts, natural products, and amino acids exhibiting both reducing and capping agent properties for the synthesis of AuNPs.[40] Earlier, our group reported the synthesis of AgNPs and AuNPs using naturally occurring sodium salt of taurocholate (NaTC) and glycocholate (NaGC) as reducing and capping agents with tunable longitudinal plasmon resonance.[41] These aspects encourage us to study and to report on possibility of green synthesis of AgNPs and AuNPs involving AA as the capping agent under sunlight irradiation. Solar energy is an external stimulus employed to control the switchable behavior of NPs, which can be used as a thermal energy substitute. Solar irradiation is the well-known largest source of carbon neutral renewable energy, which is nontoxic, nonpolluting, and traceless in chemical processes. There are reports available on the utilization of natural ambient sunlight for the synthesis of NPs.[42−47] More recently, we reported a rapid synthesis of AgNPs using the sodium salt of *N*-cholyl amino acids as the reducing and capping agents under ambient conditions in the presence of sunlight irradiation.[48]

Heavy metals like Li^+, Na^+, K^+, Mg^{2+}, Ca^{2+}, Ba^{2+}, Ni^{2+}, Cu^{2+}, Fe^{2+}, Fe^{3+}, Cr^{6+}, Zn^{2+}, Co^{2+}, Cd^{2+}, Pb^{2+},Cr^{3+}, Hg^{2+}, and Mn^{2+} are reported to be potential environmental pollutants as many of them are toxic even at trace ppm level concentrations. Therefore, determination of toxic metals in the biological system and aquatic environment has become a vital need for remedial processes. So far, there are several reports available for the detection of heavy metal ions using various analytical instruments.[49−51] Although those methods offer excellent sensitivity and multi-element analysis, they are not cost effective, involve time-consuming procedures, and are skill dependent and use nonportable accessories. In recent years, AgNPs and AuNPs have been extensively used for colorimetric detection of heavy metal ions due to their tunable size and distance-dependent optical properties with high extinction coefficients at the visible region. Advantages of using NPs as colorimetric sensors are proven to be a promising approach for simple and cost-effective protocols with high sensitivity and rapid tracking of valuable and toxic metal ions in environmental samples/systems.[49−54] So far, there are several reports available for the detection of environmentally toxic metal ions (Hg^{2+}, Pb^{2+}, and Mn^{2+}) using NPs of metal ions. For instance, Wang et al. reported the detection of Hg^{2+} ions with the naked eye using unmodified AgNPs and mercury-specific oligonucleotides as sensors.[55] Senapati et al. reported detection of Hg^{2+} using popcorn-shaped gold nanoparticles protected by tryptophan as a probe with selectivity .[56] Recently, Farhadi and co-workers reported the use of green synthesized and unmodified AgNPs for Hg^{2+} detection.[57] Chai and co-workers reported colorimetric detection of Pb^{2+} using glutathione functionalized AuNPs.[58] AuNPs generated through sunlight irradiation were used as an ultrasensitive probe for the detection of Pb^{2+} ions.[59] Metal nanoparticles have been utilized for naked eye detection of lead ions in aqueous media.[60] Recently, Zhou and co-workers reported colorimetric detection of Mn^{2+} using AgNPs cofunctionalized with 4-mercapto benzoic acid and melamine as a probe.[61] Hence, in the present investigation, we report a simple and green synthesis of AgNPs and AuNPs using L-tyrosine as capping and reducing agents under sunlight irradiation at basic pH. The prepared NPs are characterized using various instrumental techniques and are found with good water dispersibility, biocompatibility, and stability up to six months. Also, they offer the possibility to be a potential colorimetric sensors for the detection of Hg^{2+}, Pb^{2+}, and Mn^{2+} ions in aqueous medium.

MATERIALS AND METHODS

Instruments. UV−visible spectroscopy measurements were carried out on Techcomp UV-2301 spectrophotometer operated at a resolution of 1 nm. High-resolution transmission electron microscopic (HR-TEM) images were recorded with a JEOL JEM 2100 equipped with a Gatan imaging filter. The HR-TEM analysis were conducted by placing a drop of the nanoparticle solution on carbon-coated copper grid and followed by solvent evaporation under vacuum as per manual instructions. Dynamic light scattering (DLS) measurements were performed for colloidal solutions using Nanotrac Ultra NPA 253 from Microtrac, U.S.A. Cyclic voltammograms (CV) were recorded using a computer-controlled 400A electrochemical analyzer at a scan rate of 25 mV/s. A glassy carbon electrode (2 mm in diameter) was used as a working electrode, and the surface of the electrode was polished with alumina powder (0.05 μm) and rinsed well with double-distilled water before use. A platinum wire was employed as an auxiliary electrode. All the potentials were recorded with respect to a saturated calomel electrode (SCE) as the reference electrode. The FT-IR spectra were recorded using a Perkin-Elmer FT-IR (Spectrum one) spectrometer with 1 cm^{-1} resolution with KBr pellets. AgNPs solutions were centrifuged at 10,000 rpm for 30, min and the residue was dried and used in measurements. The wide-angle X-ray diffraction (WAXD) patterns of the dry powders were collected in a Philips powder diffraction apparatus (model PW 1830). The powders were taken in a glass slide, and the diffractograms were recorded using nickel-filtered Cu Kα radiation at a scanning rate of 0.6° 2θ/min.

Materials. L-Tyrosine, silver nitrate ($AgNO_3$), and hydrogen tetrachloroaurate trihydrate ($HAuCl_4.3H_2O$) were purchased from Sigma Aldrich, India. Salts of the different cations for the study [LiCl, NaCl, KCl, $MgCl_2$, $CaCl_2$, $BaCl_2$, $ZnCl_2$, $CoCl_2$, $NiCl_2$, $CdCl_2$, $HgCl_2$, $CuCl_2$, $MnSO_4$, $Pb(NO_3)_2$, $FeSO_4$, $FeCl_3$, K_2CrO_4, and $Cr(NO_3)_3$] were procured from SRL chemicals Pvt. Ltd., India. All heavy metal salt solutions (1×10^{-5} M) used for the experiments were prepared by mixing the required amount of salt in triple-distilled water, and pH was adjusted with 1N HCl and 1N NaOH. The glasswares were washed with aqua-regia (HCl: HNO_3 = 3:1 (v/v)) and rinsed well with triple-distilled water prior to use.

Synthesis of AgNPs and AuNPs. Stock solutions of $AgNO_3$ (1.0×10^{-3} M), $HAuCl_4$ (1.0×10^{-3} M), and L-tyrosine (1×10^{-2} M) were prepared using triple-distilled water, and the subsequent dilutions were made from the stock solution. In order to optimize the reaction condition, 0.3 mL of 1×10^{-3} M aqueous metal ion (M^+) solution was added to different concentrations of L-tyrosine (3.3×10^{-4} to 3.3×10^{-3} M), and the final volume was made up to 3 mL. The mixture was

kept under ambient sunlight irradiation for 5 min. The changes are found in the color of the solution, which was from colorless to lemon yellow for AgNPs and pink for AuNPs. In the case of AgNPs, the peak at 420 nm along with a weak shoulder at 330 nm were detected. The formation of the metal NPs can be attributed to the direct redox reaction between L-tyrosine and metal ions. Control experiments performed at room temperature, under UV light irradiation, sunlight irradiation, and heating at 60 °C showed that the reaction under sunlight irradiation produced a narrow SPR peak with high intensity (Figures S1and S2, Supporting data). This may be attributed to the acceleration of rate of the electron transfer to the metal ions at a comparatively faster rate.[44] Under sunlight irradiation, metal atoms are formed rapidly from the Ag^{+}/Au^{3+} ions, and the generated atoms nucleate and further grow to form NPs. Tyrosine serves as an effective capping as well as reducing reagent and helps to control the uncontrolled growth of NPs to bigger sizes. The synthesized AgNPs and AuNPs showed characteristic absorption SPR peaks at 408 and 522 nm, respectively.

RESULTS AND DISCUSSION

Effect of L-Tyrosine Composition on the Formation of AgNPs and AuNPs. As mentioned in the Materials and Methods section, the reaction was demonstrated by addition of 1.0×10^{-3} M of $AgNO_3$ ions to various concentrations of L-tyrosine ranging from 3.3×10^{-4} M to 3.3×10^{-3} M in aqueous medium under ambient sunlight irradiations. The colorless solution gradually changed to intense yellow during the formation of AgNPs depending on the concentration of L-tyrosine used in the reaction mixture. The reaction was completed within 5 min, and no change in the color was noted, indicating the reduction of Ag^{+} ions to AgNPs. The formation of AgNPs was further confirmed by the UV–visible spectra, as shown in Figure 1(a). The characteristic SPR band of the

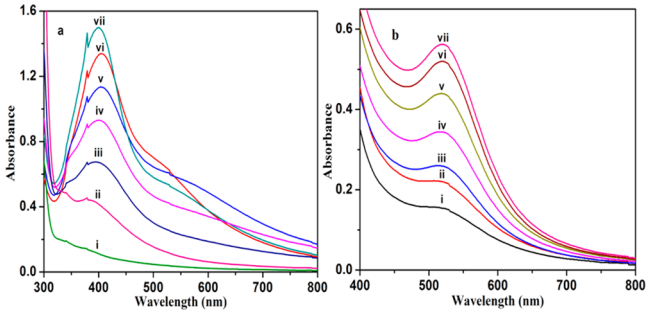

Figure 1. UV–visible spectra of L-tyrosine-stabilized AgNPs (a) and AuNPs (b) solutions at various concentrations of L-tyrosine ranging from 3.3×10^{-4} M to 3.3×10^{-3} M.

solution observed at 408 nm increased with an increase in the concentration of L-tyrosine, which may be due to the formation of spherical-shaped AgNPs.

However, at higher concentration of tyrosine (2.3×10^{-3} M to 3.3×10^{-3} M), a shoulder was noted at a longer wavelength region (520–600 nm) as shown in curves iv–vii of Figure 1(a), indicating the formation of either larger spherical particles or anisotropy ellipsoids/rods of the AgNPs. Similar conditions were used for the synthesis of AuNPs, and their resulting spectra are shown in Figure 1(b). The colorless solution gradually changed to intense pink depending upon the concentration of L-tyrosine used in the reaction mixture. The SPR peaks confirm the reduction of Au^{3+} ions to AuNPs. The reaction was completed within 5 min, and no change in the color of the solution was noted thereafter. The intensity of the SPR band at 522 nm increased without any shift in the λ_{max} with increase in the concentration of L-tyrosine from 1.3×10^{-3} M to 3.3×10^{-3} M. The prepared NPs were found stable for more than six months without any precipitation. The size and shape of the AgNPs and AuNPs prepared using two different concentrations of L-tyrosine (1.6×10^{-3} M and 3.3×10^{-4} M) are confirmed by TEM and DLS analysis. The TEM images and DLS results revealed spherical particles and with sizes dependent on the concentration of AA used (Figure 2(a–d).

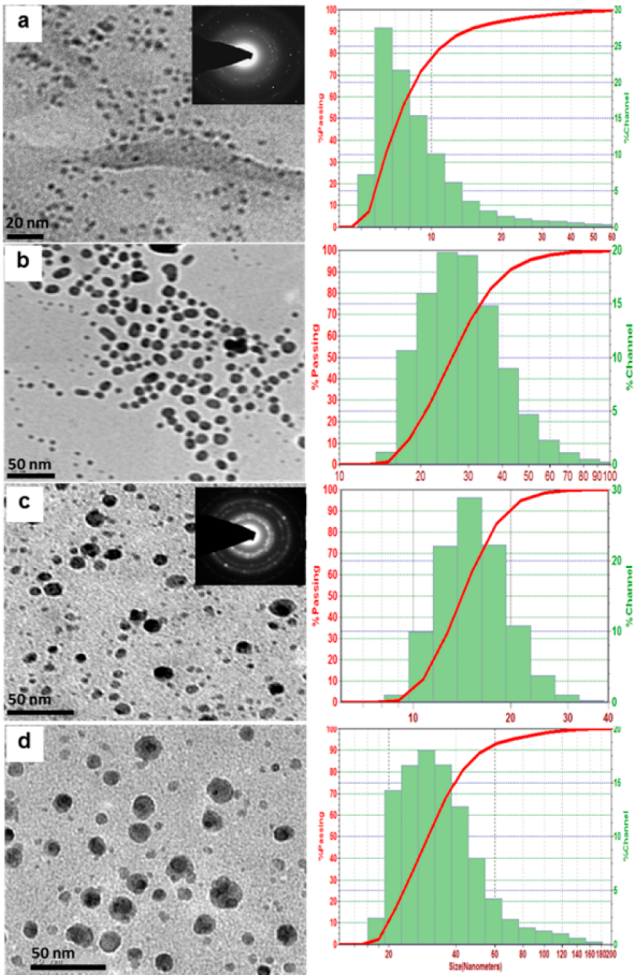

Figure 2. TEM images and corresponding particle size distribution of AgNPs and AuNPs using two different concentrations of L-tyrosine (1.3×10^{-3} and 3.3×10^{-4} M). The insets of (a) and (c) show the SAED pattern of the corresponding NPs.

The average particle size observed for AgNPs is 8.2 ± 2 nm at higher concentration and 32 ± 2 nm at lower concentration of AA. Regarding AuNPs, 17 ± 2 and 36 ± 2 nm, respectively, are detected. The XRD patterns of as prepared AgNPs and AuNPs are shown in Figure S3 of the Supporting Information. The peaks at 2θ = 38.3, 44.6, 64.7, and 77.5 are indexed as (111), (200), (220), and (311) planes for AgNPs and AuNPs, respectively. These results agree well with the reported standards (JCPDS file no. 04-0784). It shows that the prepared AgNPs and AuNPs are polycrystalline. In higher concentrations of L-tyrosine, the NPs are smaller in size, and the corresponding spectra showed a narrow SPR band with high intensity. At lower concentrations, the NPs are larger in size, and their

dx.doi.org/10.1021/sc400500z | ACS Sustainable Chem. Eng. 2014, 2, 887–896

corresponding spectrum showed a broad SPR band in a longer wavelength region.

Effect of pH on Ag and AuNPs Formation. L-Tyrosine contains three functional groups, hydroxyl (−OH), amine ($-NH_2$), and carboxylate (−COO−), that are sensitive to pH variation and act as active sites for adsorption on the surface of the NPs and stabilizes the NPs. The effect of pH on the interaction between L-tyrosine and metal salts was studied at different pH values, ranging from 7.0 to 12.0, under sunlight irradiation as shown in Figure 3. The intensity of the SPR band

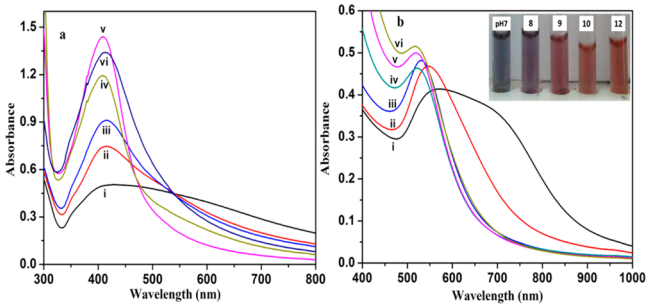

Figure 3. UV−visible spectra of L-tyrosine-stabilized AgNPs (a) and AuNPs (b) synthesized under sunlight irradiation for 5 min at different pH: (i) 7, (ii) 8, (iii) 9, (iv) 10, (v) 11, and (vi) 12. Inset shows the color photograph of the corresponding solutions.

of AgNPs increased significantly with increase in pH from neutral to alkaline medium and showed maximum intensity at pH 11.0. With further increase in pH, the SPR intensity decreased remarkably due to the formation of metal hydroxides (Figure 3a). No SPR band was observed at pH below 6, indicating that the acidic pH does not favor AgNPs formation. Figure 3b shows a typical UV−visible spectrum of the prepared AuNPs colloidal solution at different pH values, ranging from 7.0 to 12.0, in the presence of sunlight irradiation. At neutral pH, the SPR band of AuNPs with a low absorbance band at 550 nm and a shoulder peak in the longer wavelength region between 680 and 720 nm are detected.

However, the intensity of the SPR band of AuNPs increased significantly with a blue shift with an increase in the pH from neutral to alkaline, and the maximum intensity of the SPR peak was present at pH 12.0 (Figure 3b). This phenomenon indicated smaller aggregates of the AuNPs in acidic pH while stable dispersion was noted in alkaline pH. The result was in accordance with the previous reports.[62] The differences in the peak intensity and the width of the SPR band observed at various pH could be attributed to the dissociation constant of the functional groups such as $-NH_2$, −OH, and −COO− of the L-tyrosine falling within the pH values between 9.0 and 11.0. The change in color of the solutions from turbid yellow to deep yellow for AgNPs and blue to red for AuNPs was noted to identify these processes.

Cyclic Voltammetry and FT-IR Studies of L-Tyrosine-Capped Metal NPs. The electrochemical behaviors of L-tyrosine-stabilized AgNPs and AuNPs are studied by cyclic voltammetry technique using a platinum electrode with a fresh surface at a scan rate of 25 mV s^{-1}. The inset of Figure 4 (curves a,b) shows the cyclic voltammograms of 1×10^{-3} M of $AgNO_3$ and $HAuCl_4$ ions in aqueous medium. The peak potentials observed at 0.54 and 0.25 V correspond to the oxidation and reduction potential of $AgNO_3$, respectively, and the peak at 0.85 V corresponds to the stable irreversible

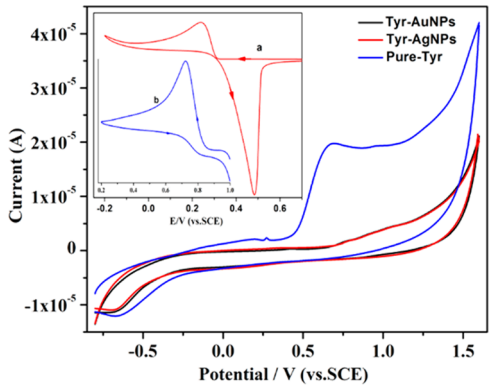

Figure 4. Cyclic voltammograms of L-tyrosine-reduced Ag and AuNPs determined at a glassy carbon electrode using 1×10^{-3} M of a supporting electrolyte (KNO_3). Curves a and b are 1×10^{-3} M of $AgNO_3$ and $HAuCl_4$ ions with a supporting electrolyte, respectively. The curve in blue is for 1×10^{-3} M of pure L-tyrosine with a supporting electrolyte, and the curves in red and black are L-tyrosine-reduced Ag and AuNPs, respectively. Scan rate: 25 mV/s.

reduction potential of the $HAuCl_4$ ions. The direct electro-oxidation of L-tyrosine at the GCE (glassy carbon electrode) gave a poorly behaved irreversible voltammogram with an anodic peak at 0.68 V, representing a very slow oxidation process at the electrode surface. The oxidation and reduction peak potentials of metal ions completely vanished, which clearly indicates the reduction of $AgNO_3/HAuCl_4$ to zero oxidation state in the form of AgNPs and AuNPs (Figure 4). This might be due to the electron donating $-NH_2$ and −OH groups of tyrosine, which act as the reducing functional groups in the formation of NPs.

The interaction of L-tyrosine on the surface of the metal NPs was confirmed by FT-IR characterizations of the as-synthesized AgNPs and AuNPs compared with pure L-tyrosine as shown in Figure 5. The broad band centered at 3217 cm^{-1} arises due to

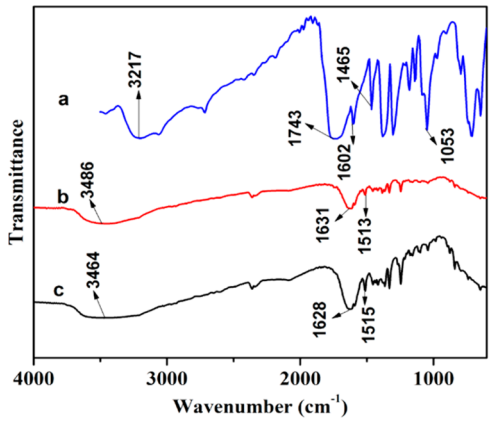

Figure 5. FT-IR spectra of (a) pure L-tyrosine, (b) L-tyrosine-stabilized AgNPs, and (c) L-tyrosine-stabilized AuNPs.

the presence of $-NH_2$ and −OH groups in the amino acid. The peaks observed at 1743, 1602, and 1465 cm^{-1} correspond to the stretching modes of the −C═O, $-NH_2$, and −COO− group, respectively, which are merged together and exhibited as a single peak at 1636 cm^{-1} after the reduction to the metal atoms. This could be due to the contribution of the $-NH_2$ and −COO− groups for the reduction and stabilization of AgNPs and AuNPs. The disappearance of the −OH stretching mode

dx.doi.org/10.1021/sc400500z | ACS Sustainable Chem. Eng. 2014, 2, 887−896

around 2500−3300 cm^{-1} in the FT-IR spectrum supports the oxidation of the phenolic group in tyrosine, which is in agreement with the earlier report.[62] The broad band appearing at 3400 cm^{-1} may be due to the existence of water molecules in the AgNPs and AuNPs as shown in curves b and c of Figure 5.

Metal Ions Recognition Ability of AgNPs. The optimized concentration of L-tyrosine (1.6×10^{-3} M)-stabilized AgNPs in the present study was tested for their application as a colorimetric sensor for detection of metal ions. The metal ions detection ability of L-tyrosine-capped AgNPs was studied separately for each of the metal ions involving Li^+, Na^+, K^+, Mg^{2+}, Ca^{2+}, Ba^{2+}, Ni^{2+}, Cu^{2+}, Fe^{2+}, Fe^{3+}, Cr^{6+}, Zn^{2+}, Co^{2+}, Cd^{2+}, Pb^{2+},Cr^{3+}, Hg^{2+}, and Mn^{2+} at a fixed concentration of 200 μL of a 1×10^{-5} M metal ion solution being added to the AgNPs solution. The change in the intensity of absorbance was monitored using UV−visible spectroscopy as shown in Figure 6. Upon addition of various metal salts (Li^+, Na^+, K^+, Mg^{2+}, Ca^{2+}, Ba^{2+}, Ni^{2+}, Cu^{2+}, Fe^{2+}, Fe^{3+}, Cr^{6+}, Zn^{2+}, Co^{2+}, Cd^{2+}, Pb^{2+}, and Cr^{3+}) to the AgNPs solution, the intensity of the SPR band showed a slight change, while the color of the solution remained constant (Figure 6a,b). However, a remarkable change in the intensity of the SPR band was observed when Hg^{2+} and Mn^{2+} were added, and the color of the solution changed from yellow to colorless for Hg^{2+} and brown for Mn^{2+}, each demonstrating the high sensitivity and selectivity of AgNPs toward Hg^{2+} and Mn^{2+}. Figure 6c demonstrates the change in absorbance intensity after the addition of different metal ions to the AgNPs solution.

The quantitative assessment of the selectivity of Hg^{2+} and Mn^{2+} ions detection was studied by changing the concentrations of these metal ions to the AgNPs at similar laboratory conditions. The SPR band of the system was monitored by UV−visible spectroscopy, and the results are shown in Figure 7. The addition of Hg^{2+} ions to the AgNPs solutions led to the gradual hypsochromic shift in its SPR band as shown in Figure 7a. The extent of the shift toward the lower wavelength region depends on the concentration of Hg^{2+} ions in the solution. This could be due to the direct redox reaction between zero valent Ag and Hg^{2+} ions, where the AgNPs oxidized to form Ag^+ and Hg^{2+} ions were reduced to a Hg atom. Further, it was confirmed by TEM analysis that there were no NPs observed after the addition of Hg^{2+} in the AgNPs solutions (Figure S4, Supporting Information). Similar observations have been reported in earlier studies on the interaction of Hg^{2+} with colloidal AgNPs.[63] However, the absorbance intensity decreased with increased concentration of Hg^{2+} ions ranging from 16 nM to 660 nM, and the value of the linear regression coefficient (R^2) was found to be 0.9970 with the detection limit up to 16 nM (inset in Figure 7a).

Similarly, quantitative Mn^{2+} assays for direct colorimetric visualization were done by adding various concentrations of Mn^{2+} to the AgNPs solution, and the changes in the SPR band were noted using UV−visible spectroscopy. As shown in Figure 7b, with increasing concentration of Mn^{2+}, there was a gradual shift observed in the SPR band of AgNPs toward a longer wavelength, indicating the aggregation of the particles, and the color of the solution changed from light yellow to brown (Figure 6c, inset). This may be due to the formation of a chelation complex between L-tyrosine-containing functional groups (−COO−, $-NH_2$, and −OH) on the NPs surface with Mn^{2+} under alkaline conditions. Also the Mn^{2+} ions rapidly induced the aggregation of AgNPs, which was confirmed by DLS analysis in the present study (Figure S5, Supporting

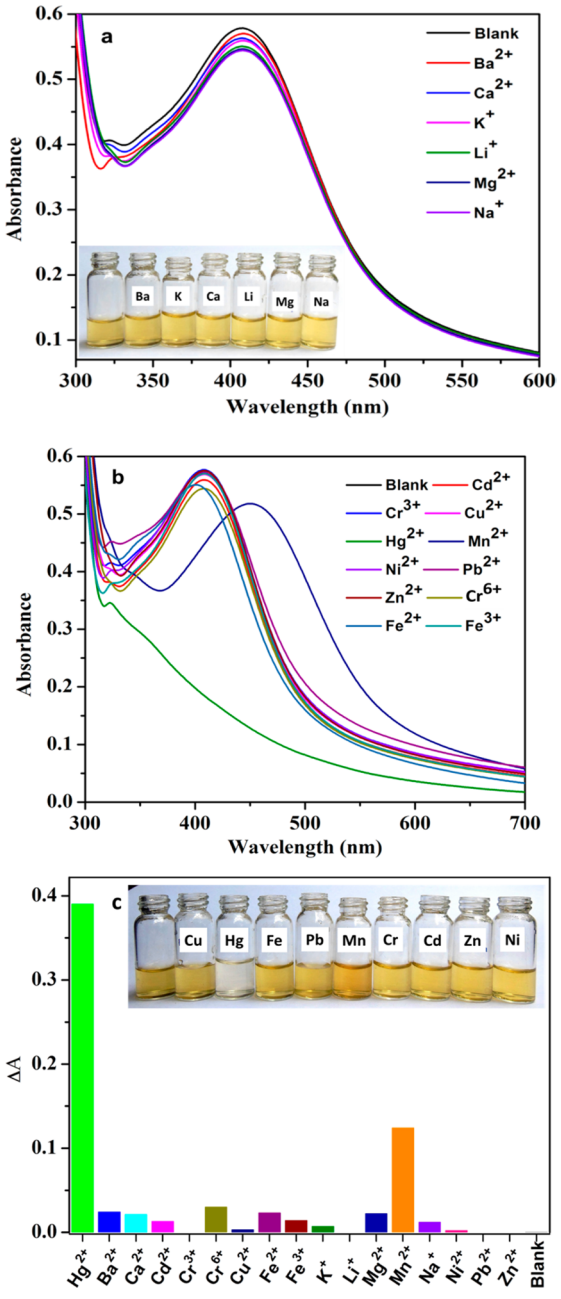

Figure 6. UV−visible absorbance spectra of L-tyrosine-stabilized AgNPs with alkali and alkaline earth metal ions (a) and transition metal ions (b). The bars and photograph represent the colorimetric response of AgNPs incubated with various metal ions (c).

Information). The observation was in agreement with the earlier reports.[64] The inset of Figure 7b shows an increase in the absorbance intensity ratio (A_{520} /$A_{408\ nm}$) with increasing concentration of Mn^{2+} ranging from 16×10^{-9} M to 50×10^{-8} M, and the value of linear regression coefficient (R^2) was found to be 0.9952 with the lowest detection limit of 16 nM.

We also performed experiments to analyze the competitive interaction of both metal ions (Mn^{2+} and Hg^{2+}) with the AgNPs solution at optimum pH conditions, and the change in the optical absorbance was noted (Figure S6a, Supporting Information). The intensity of the SPR band decreases remarkably with a hypsochromic shift in the λ_{max} and showed preferably strong interactions between Hg^{2+} and AgNPs when compared to that of Mn^{2+} and AgNPs.

dx.doi.org/10.1021/sc400500z | ACS Sustainable Chem. Eng. 2014, 2, 887−896

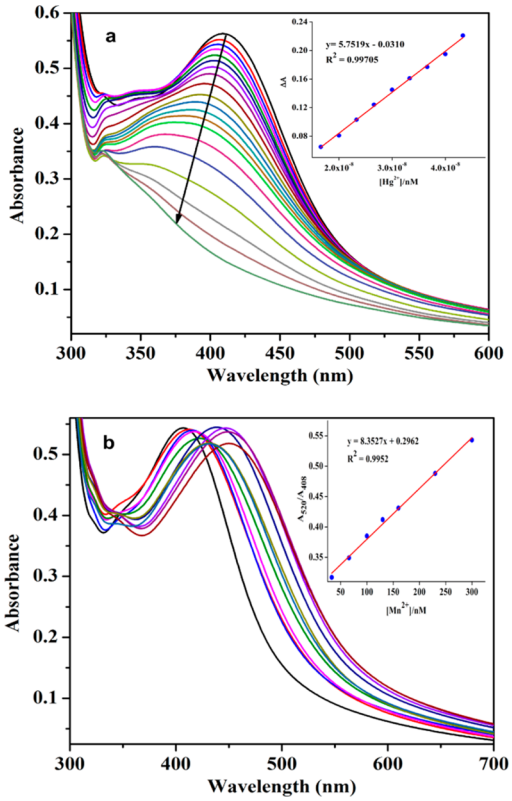

Figure 7. Stacked UV−visible spectrum of AgNPs as a function of various concentrations of (a) Hg^{2+} and (b) Mn^{2+} ions. Insets of a and b show plots of absorbance intensity of AgNPs at 408 nm vs Hg^{2+} concentration and the absorption ratios $A_{520}/A_{408\ nm}$ of AgNPs versus Mn^{2+} concentration, respectively.

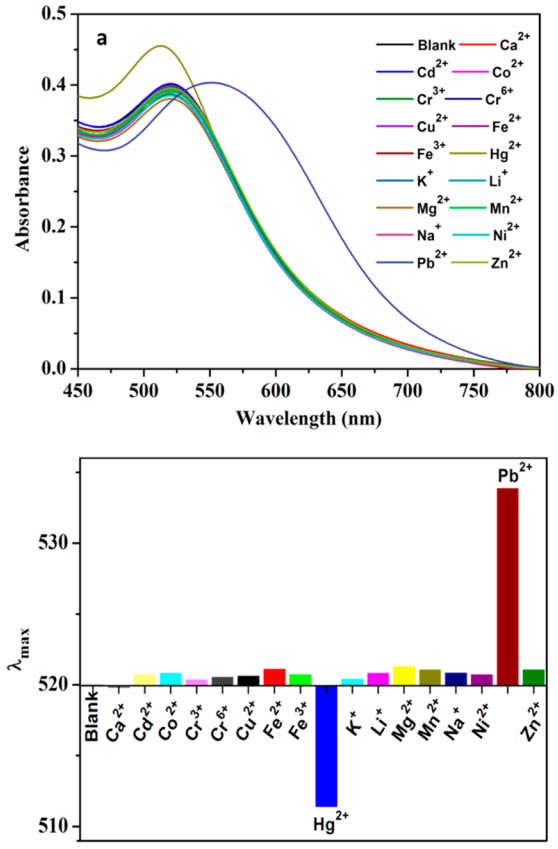

Figure 8. Absorbance spectra of L-tyrosine-stabilized AuNPs on interacting with different metal ions (a). The bars represent the colorimetric response of AuNPs incubated with various metal ions (b).

Metal Ions Recognition Ability of AuNPs. The metal ions detection ability of L-tyrosine-capped AuNPs was studied using several metal ions such as Li^{+}, Na^{+}, K^{+}, Mg^{2+}, Ca^{2+}, Ni^{2+}, Mn^{2+}, Cu^{2+}, Fe^{2+}, Fe^{3+}, Cr^{6+}, Zn^{2+}, Hg^{2+}, Co^{2+}, Cd^{2+}, Pb^{2+}, and Cr^{3+} at a fixed concentration of 100 μL of a 1×10^{-5} M solution of the metal ion to the constant composition of the AuNPs solution, and the change in the SPR intensity values are recorded as shown in Figure 8a and b. The metal ions other than Hg^{2+} and Pb^{2+} did not show any significant shift in the SPR band, and the color of the solution remained pink. Many authors have reported on the colorimetric detection of Hg^{2+} using AuNPs as the sensor in aqueous medium,[63−68] and all the studies were based on the shift of the SPR peak toward a longer wavelength due to the binding of Hg^{2+} on the AuNPs surface, which led to a color change from pink to violet.

In contrast to earlier reports, in the present study, a blue shift in the SPR peak of AuNPs was observed with an increase in concentration of the Hg^{2+}, and the color of the solution remained constant. In this report, different concentrations of aqueous solutions of Hg^{2+} ranging from 16 nM to 330 nM were analyzed, and the change in the SPR band was recorded. A significant shift in the SPR band from 522 to 511 nm was observed on increasing the concentrations of Hg^{2+} ions as shown in Figure 9a. The AuNPs did not show any major shift in the SPR maxima on increasing the concentration to 300 nM of Hg^{2+}, and no change in color was noted. The adsorption of Hg^{2+} on the surface of AuNPs leading to the formation of the core shell structure that prevented the aggregation of NPs may be the possible reason, and the size of the Hg^{2+}-adsorbed NPs was further confirmed by DLS analysis (Figure S7, Supporting Information). The result was in agreement with the reports by Morris et al. and Radhakumary et al.[67,68] Our findings were similar to the above reports, where the absorbance ratio ($A_{511}/A_{522\ nm}$) was found to vary almost linearly with an increase in the concentration of Hg^{2+} ion from 33 to 300 nM, and the value of linear regression coefficient (R^2) was found to be 0.9902 with a detection limit of 53 nM.

The colorimetric detection ability of Pb^{2+} ions were analyzed in the present study, and it was observed that the increase in concentration of Pb^{2+} from 16 to 330 nM showed the λ_{max} of the SPR band shift from 522 to 552 nm along with the change in color of the solution from pink to violet. These observations could be used for the quantitative measurement of the Pb^{2+} ion in the solution (Figure 9b). A linear correlation between the absorbance ratio ($A_{600}/A_{522\ nm}$) and the Pb^{2+} concentration (ranging from 16×10^{-9} to 100×10^{-9} M) with a linear coefficient of 0.9964 was useful for the quantitative determination of 16 nM of Pb^{2+} in aqueous solution. The stimulation of Pb^{2+} ions for the aggregation of AuNPs was confirmed by DLS analysis (Figure S8, Supporting Information). We also demonstrated experiments to analyze the competitive interaction of both metal ions (Hg^{2+} and Pb^{2+}) with the AuNPs solution at optimum conditions, and the change in the absorption intensity was noted (Figure S6b, Supporting Information). The intensity of the SPR band decreases remarkably with a small bathochromic shift in the SPR λ_{max} that showed preferably a strong interaction between Pb^{2+} and AuNPs when compared to that of Hg^{2+} and AuNPs. Hence, the method proposed in the present study is

dx.doi.org/10.1021/sc400500z | ACS Sustainable Chem. Eng. 2014, 2, 887−896

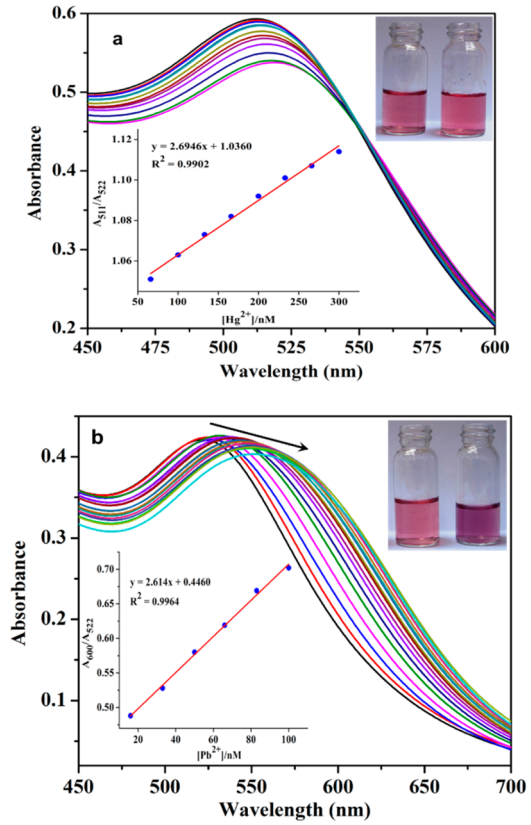

Figure 9. UV−visible spectra of AuNPs after the addition of various concentrations of (a) Hg^{2+} and (b) Pb^{2+} ions. The inset shows the plot of absorbance ratios of AuNPs versus Hg^{2+} and Pb^{2+} concentrations.

comparable with other colorimetric methods reported for the detection of Hg^{2+}, Pb^{2+}, and Mn^{2+} in aqueous solution, and the results are shown in Table S9 of the Supporting Information. The method adopted in the present study showed a lower detection limit than the reported values.

Practical Application. The colorimetric sensor application of the synthesized metal NPs was tested in real samples such as tap water and drinking water. Different concentrations of metal ions (Hg^{2+}, Mn^{2+} and Pb^{2+}) were added to the tap and drinking water, and the ability of the NPs to detect these metal ions present in the water samples was analyzed. A linear increase in the absorption intensity of AgNPs at 408 nm was observed at a concentration of Hg^{2+} ranging between 20 and 150 nM (Figure S10a, Supporting Information). The lowest detectable concentrations of Hg^{2+} in drinking water and tap water were estimated to be 19 and 26 nM, respectively. The absorption ratio ($A_{520}/A_{408\ nm}$) of AgNPs showed a linear increase with Mn^{2+} concentration in drinking and tap water ranging between 20 and 200 nM (Figure S10b, Supporting Information). The lowest detectable concentrations of Mn^{2+} in drinking water and tap water were estimated to be 23 and 26 nM, respectively. Similarly, the absorption ratio ($A_{522}/A_{511\ nm}$) of AuNPs increased linearly with an increase in concentration of Hg^{2+} in drinking water and tap water ranging between 60 and 200 nM, and the lowest detectable concentration of Hg^{2+} in drinking water and tap water samples were estimated to be 60 and 72 nM, respectively (Figure S11a, Supporting Information). The absorption ratio ($A_{600}/A_{522\ nm}$) of AuNPs also showed a linear increase in detecting Pb^{2+} ions in the drinking water and tap water over a concentration range between 20 and 100 nM, and the detectable lowest concentration of Pb^{2+} was estimated to be 23 and 26 nM drinking water and tap water samples, respectively (Figure S11b, Supporting Information). The metal ion detection ability of the AgNPs and AuNPs was significantly different when tested with drinking water and tap water in comparison to that of distilled and demineralized water. This may be due to the presence of some impurities in drinking water and tap water that could influence the detection ability of metal NPs.

Possible Mechanism for NPs Interaction with the Heavy Metal Ions. On the basis of the present study and earlier reports, we propose a possible mechanism for the interaction of Ag and AuNPs with heavy metal ions, which is

Scheme 1. Schematic Illustration of the Formation Process of Ag and AuNPs and Its Interaction with Metal Ions

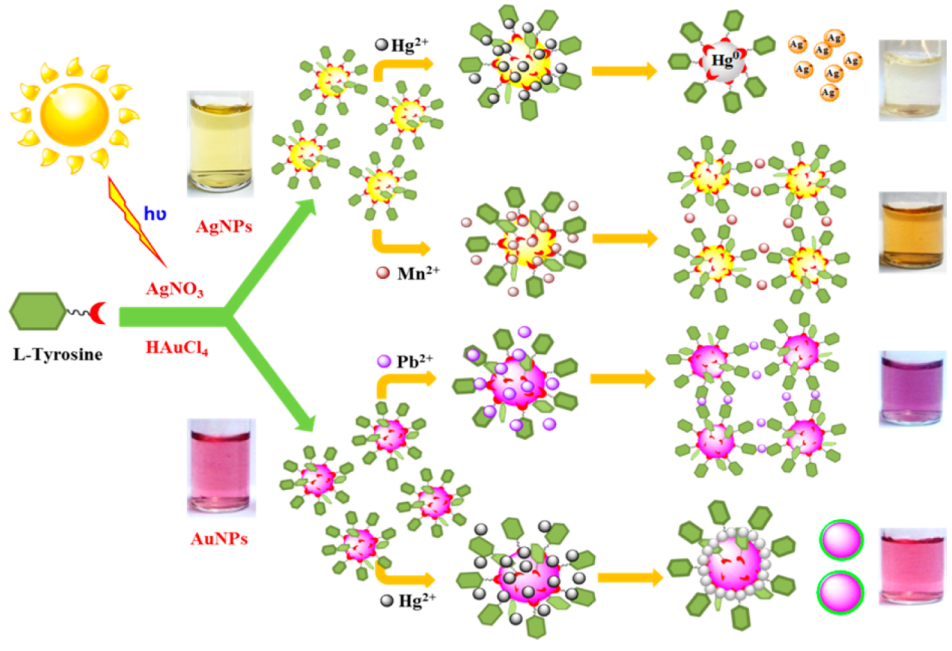

dx.doi.org/10.1021/sc400500z | ACS Sustainable Chem. Eng. 2014, 2, 887−896

shown in Scheme 1. In the present study, we observed a blue shift on increasing the concentration of Hg^{2+} ions added to the AgNPs solution, and the color of the solution changed from yellow to colorless. This could be due to the oxidation of Ag^0 to Ag^+ during the process of reduction of Hg^{2+} ions.[57] The decrease in the intensity of the SPR band with a blue shift could be due to either the influence of Hg^{2+} ions on the surface of AgNPs with or without amalgamation or reduction in the size of the AgNPs. Morris et al.[67] and Radhakumary et al.[68] reported that the interaction of AuNPs with Hg^{2+}, resulted in a blue shift in the SPR band that could be due to the formation of a core shell structure. Our observations were similar to their report. The intensity of the SPR band shifted toward a lower wavelength, and the color of the solution remained the same with an increase in concentration of Hg^{2+}. This may be due to the adsorption of Hg^{2+} ions on the surface of the AuNPs forming a core shell structure, and this observation further supports that these NPs do not aggregate together. However, after interaction of Mn^{2+} with AgNPs and Pb^{2+} with AuNPs, a red shift in the SPR band was observed along with an increase in the concentration of these metal ions. This could be due to the complexing action of L-tyrosine present on the surface of NPs and metal ions (Pb^{2+} or Mn^{2+}), which leads to the aggregation of NPs.

CONCLUSIONS

In conclusion, the present study reports the simple and green approach for the synthesis of AgNPs and AuNPs using L-tyrosine under ambient sunlight irradiation in aqueous medium, and NPs were characterized by UV−visible, HR-TEM, DLS, cyclic voltammetry, and FT-IR techniques. L-Tyrosine acted as both reducing and capping agents for the stabilization of metal NPs, and the particles were stable for up to six months. The −OH and $-NH_2$ groups of L-tyrosine were found to be involved in the reduction of the metal ions, while the −COO− group binds strongly to the surface of the NPs. The size of the metal NPs could be controlled by varying the concentrations of capping agent and pH of the reaction medium. The synthesized NPs were used as colorimetric sensors for detection of various heavy metals in aqueous medium. The prepared AgNPs were highly sensitive to Hg^{2+} and Mn^{2+} ions, while AuNPs were highly sensitive to Hg^{2+} and Pb^{2+} ions. These colorimetric sensors could be used in both quantitative and qualitative detection of metal ions such as Hg^{2+}, Pb^{2+}, and Mn^{2+} ions with the detection limits of nM concentration and also could be easily visualized with the naked eye or by using a UV−visible spectrometer. We validated the practicality of this method through the analyses of drinking water and tap water samples. This simple, rapid, and cost-effective sensing system appears to hold great practicality for the detection of heavy metal ions in real samples.

ASSOCIATED CONTENT

Supporting Information

Data contains UV−visible spectrum and powder XRD and DLS analyses. This material is available free of charge via the Internet at http://pubs.acs.org.

AUTHOR INFORMATION

Corresponding Author

*E-mail: nrajendiar@yahoo.com. Tel.: +91 44 22202822.

Notes

The authors declare no competing financial interest.

ACKNOWLEDGMENTS

The authors thank the University Grants Commission (UGC) and Department of Science and Technology (DST), Government of India, for their financial support. N.R. also thanks the National Centre for Nanoscience and Nanotechnology (NCNSNT), University of Madras, for HR-TEM studies, and Metrohm India Limited, Chennai, for DLS analysis.

REFERENCES

(1) Burda, C.; Chen, X.; Narayanan, R.; El-Sayed, M. A. Chemistry and properties of nanocrystals of different shapes. *Chem. Rev.* **2005**, *105* (4), 1025−1102.
(2) Shukla, R.; Bansal, V.; Chaudhary, M.; Basu, A.; Bhonde, R. R.; Sastry, M. Biocompatibility of gold nanoparticles and their endocytotic fate inside the cellular compartment: A microscopic overview. *Langmuir* **2005**, *21* (23), 10644−10654.
(3) Liz-Marzan, L. M. Tailoring surface plasmons through the morphology and assembly of metal nanoparticles. *Langmuir* **2006**, *22* (1), 32−41.
(4) Kelly, K. L.; Coronado, E.; Zhao, L. L.; Schatz, G. C. The optical properties of metal nanoparticles: The influence of size, shape, and dielectric environment. *J. Phys. Chem. B* **2003**, *107* (3), 668−677.
(5) Nallathamby, P. D.; Lee, K. J.; Xu, X. N. Design of stable and uniform single nanoparticle photonics for in vivo dynamics imaging of nano environments of zebra fish embryonic fluids. *ACS Nano* **2008**, *2* (7), 1371−1380.
(6) Liu, P.; Zhao, M. Silver nanoparticle supported on halloysite nanotubes catalyzed reduction of 4-nitrophenol (4-NP). *Appl. Surf. Sci.* **2009**, *255* (7), 3989−3993.
(7) Flores, S. P.; Wheeler, D. A.; Tran, T. M.; Tanaka, Z.; Jiang, C.; Flores, M. B.; Qian, F.; Li, Y.; Chen, B.; Zhang, J. Z. SERS spectroscopy and SERS imaging of Shewanella oneidensis using silver nanoparticles and nanowires. *Chem. Commun.* **2011**, *47* (14), 4129−4131.
(8) Erathodiyil, N.; Ying, J. Y. Functionalization of inorganic nanoparticles for bioimaging applications. *Acc. Chem. Res.* **2011**, *44* (10), 925−935.
(9) Zhou, Y.; Kong, Y.; Kundu, S.; Cirillo, J. D.; Liang, H. Antibacterial activities of gold and silver nanoparticles against *Escherichia coli* and bacillus Calmette-Guerin. *J. Nanobiotechnol.* **2012**, *10*, 19.
(10) Shervani, Z.; Yamamoto, Y. Carbohydrate-directed synthesis of silver and gold nanoparticles: Effect of the structure of carbohydrates and reducing agents on the size and morphology of the composites. *Carbohydr. Res.* **2011**, *346* (5), 651−658.
(11) Wei, H.; Wang, Z.; Zhang, J.; House, S.; Gao, Y. G.; Yang, L.; Robinson, H.; Tan, L. H.; Xing, H.; Hou, C.; Robertson, I. M.; Zuo, J. M.; Lu, Y. Time-dependent, protein-directed growth of gold nanoparticles within a single crystal of lysozyme. *Nat. Nanotechnol.* **2011**, *6* (2), 93−97.
(12) Si, S.; Mandal, T. K. Tryptophan-based peptides to synthesize gold and silver nanoparticles: A mechanistic and kinetic study. *Chem.—Eur. J.* **2007**, *13* (11), 3160−3168.
(13) Pal, A.; Esumi, K.; Pal, T. Preparation of nanosized gold particles in a biopolymer using UV photoactivation. *J. Colloid Interface Sci.* **2005**, *288* (2), 396−401.
(14) Nadagouda, M. N.; Varma, R. S. Green and controlled synthesis of gold and platinum nanomaterials using vitamin B2: Density-assisted self-assembly of nanospheres, wires and rods. *Green Chem.* **2006**, *8* (6), 516−518.
(15) Nadagouda, M. N.; Varma, R. S. A greener synthesis of core (Fe, Cu)-shell (Au, Pt, Pd and Ag) nanocrystals using aqueous vitamin C. *Cryst. Growth Des.* **2007**, *7* (12), 2582−2587.

(16) Baruwati, B.; Polshettiwar, V.; Varma, R. S. Glutathione promoted expeditious green synthesis of silver nanoparticles in water using microwaves. *Green Chem.* **2009**, *11* (7), 926−930.
(17) Nadagouda, M. N.; Hoag, G.; Collins, J.; Varma, R. S. Green synthesis of Au nanostructures at room temperature using biodegradable plant surfactants. *Cryst. Growth Des.* **2009**, *9* (11), 4979−4983.
(18) Baruwati, B.; Varma, R. S. High value products from waste: Grape pomace extract—a three-in-one package for the synthesis of metal nanoparticles. *ChemSusChem* **2009**, *2* (11), 1041−1044.
(19) Raveendran, P.; Fu, J.; Wallen, S. L. A simple and "green" method for the synthesis of Au, Ag, and Au−Ag alloy nanoparticles. *Green Chem.* **2006**, *8* (1), 34−38.
(20) Huang, X.; Wu, H.; Liao, X.; Shi, B. One-step, size-controlled synthesis of gold nanoparticles at room temperature using plant tannin. *Green Chem.* **2010**, *12* (3), 395−399.
(21) Zou, L.; Qi, W.; Huang, R.; Su, R.; Wang, M.; He, Z. Green synthesis of a gold nanoparticle−nanocluster composite nanostructures using trypsin as linking and reducing agents. *ACS Sustainable Chem. Eng.* **2013**, *1* (11), 1398−1404.
(22) Huang, Y. F.; Lin, Y. W.; Chang, H. T. Growth of various Au−Ag nanocomposites from gold seeds in amino acid solutions. *Nanotechnology* **2006**, *17* (19), 4885−4894.
(23) Bhargava, S. K.; Booth, J. M.; Agrawal, S.; Coloe, P.; Kar, G. Gold nanoparticle formation during bromoaurate reduction by amino acids. *Langmuir* **2005**, *21* (13), 5949−5956.
(24) Si, S.; Dinda, E.; Mandal, T. K. In situ synthesis of gold and silver nanoparticles by using redox-active amphiphiles and their phase transfer to organic solvents. *Chem.−Eur. J.* **2007**, *13* (35), 9850−9861.
(25) Selvakannan, P. R.; Mandal, S.; Phadtare, S.; Gole, A.; Pasricha, R.; Adyanthaya, S. D.; Sastry, M. Water-dispersible tryptophan protected gold nanoparticles prepared by the spontaneous reduction of aqueous chloroaurate ions by the amino acid. *J. Colloid Interface Sci.* **2004**, *269*, 97−102.
(26) Sarangi, S. N.; Hussain, A. M. P.; Sahu, S. N. Strong UV absorption and emission from L-cysteine capped monodispersed gold nanoparticles. *Appl. Phys. Lett.* **2009**, *95* (7), 073109.
(27) Liu, Z.; Xing, Z.; Zu, Y.; Tan, S.; Zhao, L.; Zhou, Z.; Sun, T. Synthesis and characterization of L-histidine capped silver nanoparticles. *Mater. Sci. Eng.: C* **2012**, *32* (4), 811−816.
(28) Liu, S.; Chen, G.; Prasad, P. N.; Swihart, M. T. Synthesis of monodisperse Au, Ag and Au−Ag alloy nanoparticles with tunable size and surface plasmon resonance frequency. *Chem. Mater.* **2011**, *23* (18), 4098−4101.
(29) Liu, Z.; Zu, Y.; Fu, Y.; Meng, R.; Guo, S.; Xing, Z.; Tan, S. Hydrothermal synthesis of histidine- functionalized single-crystalline gold nanoparticles and their pH-dependent UV absorption characteristic. *Colloids Surf., B* **2010**, *76* (1), 311−316.
(30) Herbani, Y.; Nakamura, T.; Sato, S. Synthesis of near-monodispersed Au−Ag nanoalloys by high intensity laser irradiation of metal ions in hexane. *J. Phys. Chem. C* **2011**, *115* (44), 21592−21598.
(31) Hamaguchi, K.; Kawasaki, H.; Arakawa, R. Photochemical synthesis of glycine-stabilized gold nanoparticles and its heavy-metal-induced aggregation behavior. *Colloids Surf., A* **2010**, *367* (1−3), 167−173.
(32) Shao, Y.; Jin, Y.; Dong, S. Synthesis of gold nanoplates by aspartate reduction of gold chloride. *Chem. Commun.* **2004**, *9*, 1104−1105.
(33) Ma, Z.; Han, H. One-step synthesis of cystine-coated gold nanoparticles in aqueous solution. *Colloids Surf., A* **2008**, *317* (1−3), 229−233.
(34) Zaheer, Z.; Malik, M. A.; Al-Nowaiser, F. M.; Khan, Z. Preparation of silver nanoparticles using tryptophan and its formation mechanism. *Colloids Surf., B* **2010**, *81* (2), 587−592.
(35) Rafey, A.; Shrivastavaa, K. B. L.; Iqbal, S. A.; Khan, Z. Growth of Ag-nanoparticles using aspartic acid in aqueous solutions. *J. Colloid Interface Sci.* **2011**, *354* (1), 190−195.
(36) Khan, Z.; AL-Thabaiti, S. A.; Obaid, A. Y.; Khan, Z. A.; Abdulrahman Al-Youbi, A. O. Shape-directing role of cetyltrimethyl ammonium bromide in the preparation of silver nanoparticles. *J. Colloid Interface Sci.* **2012**, *367* (1), 101−108.
(37) Wangoo, N.; Bhasin, K. K.; Mehta, S. K.; Suri, C. R. Synthesis and capping of water-dispersed gold nanoparticles by an amino acid: Bioconjugation and binding studies. *J. Colloid Interface Sci.* **2008**, *323* (2), 247−254.
(38) Swami, A.; Kumar, A.; D'Costa, M.; Pasricha, R.; Sastry, M. Variation in morphology of gold nanoparticles synthesized by the spontaneous reduction of aqueous chloroaurate ions by alkylated tyrosine at a liquid−liquid and air−water interface. *J. Mater. Chem.* **2004**, *14*, 2696−2702.
(39) Selvakannan, P. R.; Mandal, S.; Phadtare, S.; Pasricha, R.; Sastry, M. Capping of gold nanoparticles by the amino acid lysine renders them water-dispersible. *Langmuir* **2003**, *19* (8), 3545−3549.
(40) Dumur, F.; Guerlin, A.; Dumas, E.; Bertin, D.; Gigmes, D.; Mayer, C. R. Controlled spontaneous generation of gold nanoparticles assisted by dual reducing and capping agents. *Gold Bull.* **2011**, *44*, 119−137.
(41) Kasthuri, J.; Rajendiran, N. Functionalization of silver and gold nanoparticles using amino acid conjugated bile salts with tunable longitudinal plasmon resonance. *Colloids Surf., B* **2009**, *73* (2), 387−393.
(42) Rastogi, L.; Arunachalam, J. Sunlight based irradiation strategy for rapid green synthesis of highly stable silver nanoparticles using aqueous garlic (*Allium sativum*) extract and their antibacterial potential. *Mater. Chem. Phys.* **2011**, *129* (1−2), 558−563.
(43) Luo, Y. Size-controlled preparation of polyelectrolyte-protected gold nanoparticles by natural sunlight radiation. *Mater. Lett.* **2007**, *61* (11−12), 2164−2166.
(44) Luo, Y. Size-controlled preparation of dendrimer-protected gold nanoparticles: A sunlight irradiation-based strategy. *Mater. Lett.* **2008**, *62* (21−22), 3770−3772.
(45) Pienpinijtham, P.; Han, X. X.; Suzuki, T.; Thammacharoen, C.; Ekgasit, S.; Ozaki, Y. Micrometer-sized gold nanoplates: starch-mediated photochemical reduction synthesis and possibility of application to tip-enhanced Raman scattering (TERS). *Phys. Chem. Chem. Phys.* **2012**, *14* (27), 9636−9641.
(46) Patil, A. B.; Patil, D. S.; Bhanage, B. M. Selective and efficient synthesis of decahedral palladium nanoparticles and its catalytic performance for Suzuki coupling reaction. *J. Mol. Catal A: Chem.* **2012**, *365*, 146−153.
(47) Yin, Y.; Liu, J.; Jiang, G. Sunlight-induced reduction of ionic Ag and Au to metallic nanoparticles by dissolved organic matter. *ACS Nano* **2012**, *6* (9), 7910−7919.
(48) Annadhasan, M.; Sankar Babu, V. R.; Naresh, R.; Umamaheswari, K.; Rajendiran, N. A sunlight-induced rapid synthesis of silver nanoparticles using sodium salt of N-cholyl amino acids and its antimicrobial applications. *Colloids Surf., B* **2012**, *96*, 14−21.
(49) Aragay, G.; Pons, J.; Merkoci, A. Recent trends in macro-, micro-, and nanomaterial-based tools and strategies for heavy-metal detection. *Chem. Rev.* **2011**, *111* (5), 3433−3458.
(50) Nolan, E. M.; Lippard, S. J. Tools and tactics for the optical detection of mercuric ion. *Chem. Rev.* **2008**, *108* (9), 3443−3480.
(51) Ray, P. C. Size and shape dependent second order nonlinear optical properties of nanomaterials and their application in biological and chemical sensing. *Chem. Rev.* **2010**, *110* (9), 5332−5365.
(52) Cao, Y. C.; Jin, R. C.; Thaxton, S.; Mirkin, C. A. A two-color-change, nanoparticle based method for DNA detection. *Talanta* **2005**, *67* (3), 449−455.
(53) Nam, J. M.; Park, S. J.; Mirkin, C. A. Bio-barcodes based on oligonucleotide-modified nanoparticles. *J. Am. Chem. Soc.* **2002**, *124* (15), 3820−3821.
(54) Lee, J. S.; Han, M. S.; Mirkin, C. A. Colorimetric detection of mercuric ion (Hg^{2+}) in aqueous media using DNA-functionalized gold nanoparticles. *Angew. Chem., Int. Ed.* **2007**, *119* (22), 4171−4174.

(55) Wang, Y.; Yang, F.; Yang, X. Colorimetric detection of mercury (II) ion using unmodified silver nanoparticles and mercury-specific oligonucleotides. *ACS Appl. Mater. Interfaces* **2010**, *2* (2), 339−342.
(56) Senapati, T.; Senapati, D.; Singh, A. K.; Fan, Z.; Kanchanapally, R.; Ray, P. C. Highly selective SERS probe for Hg(II) detection using tryptophan-protected popcorn shaped gold nanoparticles. *Chem. Commun.* **2011**, *47* (37), 10326−10328.
(57) Farhadi, K.; Forough, M.; Molaei, R.; Hajizadeh, S.; Rafipour, A. Highly selective Hg^{2+} colorimetric sensor using green synthesized and unmodified silver nanoparticles. *Sens. Actuators, B* **2012**, *161*, 880−885.
(58) Chai, F.; Wang, C.; Wang, T.; Li, L.; Su, Z. Colorimetric detection of Pb^{2+} using glutathione functionalized gold nanoparticles. *ACS Appl. Mater. Interfaces* **2010**, *2* (5), 1466−1470.
(59) Chien, Y. H.; Huang, C. C.; Wang, S. W.; Yeh, C. S. Synthesis of nanoparticles: Sunlight formation of gold nanodecahedra for ultra-sensitive lead-ion detection. *Green Chem.* **2011**, *13* (5), 1162−1166.
(60) Yoosaf, K.; Ipe, B. I.; Suresh, C. H.; Thomas, K. G. In situ synthesis of metal nanoparticles and selective naked-eye detection of lead ions from aqueous media. *J. Phys. Chem. C* **2007**, *111* (34), 12839−12847.
(61) Zhou, Y.; Zhao, H.; Li, C.; He, P.; Peng, W.; Yuan, L.; Zeng, L.; He, Y. Colorimetric detection of Mn^{2+} using silver nanoparticles co-functionalized with 4-mercaptobenzoic acid and melamine as a probe. *Talanta* **2012**, *97*, 331−335.
(62) Selvakannan, P. R.; Swami, A.; Srisathiyanarayanan, D.; Shirude, P. S.; Pasricha, R.; Mandal, A. B.; Sastry, M. Synthesis of aqueous Au core−Ag shell nanoparticles using tyrosine as a pH-dependent reducing agent and assembling phase-transferred silver nanoparticles at the air−water interface. *Langmuir* **2004**, *20* (18), 7825−7836.
(63) Rex, M.; Hernandez, F. E.; Campiglia, A. D. Pushing the limits of mercury sensors with gold nanorods. *Anal. Chem.* **2006**, *78* (2), 445−451.
(64) Chen, L.; Lou, T.; Yu, C.; Kang, Q.; Chen, L. N-1-(2-Mercaptoethyl)thymine modification of gold nanoparticles: A highly selective and sensitive colorimetric chemosensor for Hg^{2+}. *Analyst* **2011**, *136* (22), 4770−4773.
(65) Darbha, G. K.; Singh, A. K.; Rai, U. S.; Yu, E.; Yu, H.; Ray, P. C. Selective detection of mercury (II) ion using nonlinear optical properties of gold nanoparticles. *J. Am. Chem. Soc.* **2008**, *130* (25), 8038−8043.
(66) Chen, X.; Zu, Y.; Xie, H.; Kemas, A. M.; Gao, Z. Coordination of mercury (II) to gold nanoparticle associated nitrotriazole towards sensitive colorimetric detection of mercuric ion with a tunable dynamic range. *Analyst* **2011**, *136* (8), 1690−1696.
(67) Morris, T.; Copeland, H.; McLinden, E.; Wilson, S.; Szulczewski, G. The effects of mercury adsorption on the optical response of size-selected gold and silver nanoparticles. *Langmuir* **2002**, *18* (20), 7261−7264.
(68) Radhakumary, C.; Sreenivasan, K. Gold nanoparticles generated through "green route" bind Hg^{2+} with a concomitant blue shift in plasmon absorption peak. *Analyst* **2011**, *136* (14), 2959−2962.